Factors influencing ice formation and growth in simulations of a mixed-phase wave cloud

C. Dearden,[1] P. J. Connolly,[1] T. Choularton,[1] P. R. Field,[2] and A. J. Heymsfield[3]

Received 15 March 2012; revised 30 August 2012; accepted 4 September 2012; published 12 October 2012.

[1] In this paper, numerical simulations of an orographically induced wave cloud sampled in-situ during the ICE-L (Ice in Clouds Experiment - Layer clouds) field campaign are performed and compared directly against the available observations along various straight and level flight paths. The simulations are based on a detailed mixed-phase bin microphysics model embedded within a 1-D column framework with the latest parameterizations for heterogeneous ice nucleation and an adaptive treatment of ice crystal growth based on the evolution of crystal habit. The study focuses on the second of two clouds sampled on 16th November 2007, the in-situ data from which exhibits some interesting and more complex microphysics than other flights from the campaign. The model is used to demonstrate the importance of both heterogeneous and homogeneous nucleation in explaining the in-situ observations of ice crystal concentration and habit, and how the ability to isolate the influence of both nucleation mechanisms helps when quantifying active IN concentrations. The aspect ratio and density of the simulated ice crystals is shown to evolve in a manner consistent with the in-situ observations along the flight track, particularly during the transition from the mixed-phase region of the cloud to the ice tail dominated by homogeneous nucleation. Some additional model runs are also performed to explore how changes in IN concentration and the value of the deposition coefficient for ice affect the competition between heterogeneous and homogeneous ice formation in the wave cloud, where the Factorial Method is used to isolate and quantify the effect of such non-linear interactions. The findings from this analysis show that the effect on homogeneous freezing rates is small, suggesting that any competition between the microphysical variables is largely overshadowed by the strong dynamical forcing of the cloud in the early stages of ice formation.

Citation: Dearden, C., P. J. Connolly, T. Choularton, P. R. Field, and A. J. Heymsfield (2012), Factors influencing ice formation and growth in simulations of a mixed-phase wave cloud, *J. Adv. Model. Earth Syst., 4*, M10001, doi:10.1029/2012MS000163.

1. Introduction

[2] The simulation of clouds, particularly those involving the ice phase, remains a major source of uncertainty in numerical models of the Earth's atmosphere. It is well established that the lack of a standard theory of the factors controlling heterogeneous ice nucleation means that the problem of accurately quantifying ice crystal number concentrations is as much of an issue in cloud resolving modeling studies as it is in global scale modeling [*Cantrell and Heymsfield*, 2005], and that the parameterizations of active Ice Nuclei (IN) concentrations typically used in cloud and climate models [e.g., *Meyers et al.*, 1992; *Cooper*, 1986; *Fletcher*, 1962] can disagree with each other by as much as a factor of 1000 for a specified temperature. It is believed that active IN concentrations need to be predicted to within a factor of ten at worst in order to avoid significant errors in cloud microphysical processes [*DeMott et al.*, 2010], which in turn can lead to errors in climate model predictions due to the impact on the cloud radiative forcing. Thus projects such as the Ice in Cloud Experiment - Layer clouds (ICE-L) field campaign provide a much needed observational constraint which can be used to help develop and test the latest parameterization schemes describing primary heterogeneous ice formation and growth. The ICE-L campaign focused on mixed-phase lenticular wave clouds over the Rocky mountains, USA in the autumn of 2007.

[1]School of Earth, Atmospheric and Environmental Science, University of Manchester, Manchester, UK.
[2]Atmospheric Processes and Parameterization, Met Office, Exeter, UK.
[3]National Center for Atmospheric Research, Boulder, Colorado, USA.

1942-2466/12/2012MS000163

Measurements from ICE-L are particularly useful because the isolation, long lifetime and minimal turbulent mixing of the clouds in question makes them ideal natural laboratories to explore ice nucleation and subsequent growth mechanisms via in-situ measurements. Furthermore, the problem of shattering of large ice crystals on instrument inlets leading to contamination of previous IN measurements [*Eidhammer et al.*, 2010] is largely avoided in ICE-L due to the relatively small size of the ice crystals and the use of in-situ microphysics probes that were designed specifically to resist shattering. A full description of the probes used in ICE-L is given in *Heymsfield et al.* [2011] and *Field et al.* [2012].

[3] In-situ measurements from dedicated field campaigns combined with cloud resolving modeling studies together form a pathway toward increasing our knowledge of ice phase microphysical processes and thus improving our ability to represent cold clouds in weather and climate models. Indeed several modeling studies based on the ICE-L project have already led to advancements in understanding. For instance, the study by *Field et al.* [2012] used a kinematic 1-D column model framework with bulk microphysics to identify the dominant heterogeneous ice nucleation mechanisms most likely responsible for ice formation across the range of ICE-L wave clouds sampled. This was achieved through a simplified representation of the different nucleation modes combined with a prognostic IN treatment. An ensemble of model integrations were performed for a range of prognostic IN values and the simulations that gave the best agreement with the observations (in terms of the ice number concentration and the timing of the onset of ice formation) were identified. They concluded that condensation/immersion freezing gave the best agreement with the in-situ measurements. This corroborates recent results from several years of remote sensing of mid-level clouds [*Westbrook and Illingworth*, 2011] and also laboratory studies of ice nucleation on dust particles [*Connolly et al.*, 2009]. Another study by *Eidhammer et al.* [2010] focused on one particular ICE-L case study from the 18th November 2007 (RF04), and used a Lagrangian parcel model framework to demonstrate that 2 of the latest primary nucleation parameterizations were found to predict ice crystal number concentrations within the cloud to within a factor of 3 of the observations. While these modeling results represent clear progress, there are still aspects of the measurements that are not fully understood and thus warrant further modeling work to investigate, hence the motivation for this paper. For instance, in-situ measurements from the second of two clouds sampled on the 16th November (RF03) showed very different ice crystal concentrations compared to RF04, despite both clouds showing similar vertical velocities and temperatures along the flight track [*Field et al.*, 2008]. Specifically, RF03 exhibited steadily increasing ice crystal concentrations along the flight track in the mixed-phase region of the cloud, followed by a distinct ice tail where the ice concentrations jumped significantly up to around 100 L^{-1}. There are two possible explanations for this behavior:

[4] 1. The nature of the aerosol particles present in the two cases may have been different;

[5] 2. Homogeneously nucleated ice may have formed at some higher altitude in RF03 and then crossed the flight track level at some later time as the ice followed streamlines along the descending part of the wave.

[6] The out-of-cloud IN counter measurements for both cases show similar values of around 1 L^{-1} [*Field et al.*, 2012], which is too low to explain the high ice crystal concentrations in RF03 and therefore casts doubt on the first of these explanations. Both the observational study of *Pratt et al.* [2010] and the bulk modeling study of *Field et al.* [2012] have noted the potential for homogeneous freezing to occur in RF03, such that ice formed through homogeneous nucleation could fall from above into the sampling altitude and lead to an increase in ice crystal number concentrations. However, a detailed investigation of this interpretation remains lacking; further the influence of homogeneous nucleation on the evolution of the microphysics along the flight track has also not been studied. Thus the aim of this paper is to build up a comprehensive understanding of the history of the RF03 case using a 1-D column model that can advect air parcels along multiple trajectories, and to establish the key factors that affect the ability of the model to replicate the observed microphysical characteristics.

2. Model Description

[7] The model used in this paper is the recently developed University of Manchester Aerosol-Cloud-Precipitation-Interaction-Model (ACPIM), a sophisticated mixed-phase bin microphysics model that takes advantage of recent developments in the representation of ice phase processes. While the authors are aware of several existing bin microphysical simulations of the mixed-phase [*Khain et al.*, 2004; *Seifert et al.*, 2006; *Teller and Levin*, 2008], these are in relation to cases of deep convection, and the authors are not aware of any recent mixed-phase bin modeling studies in the context of layer clouds; this paper provides an opportunity to address this imbalance. The ACPIM bin microphysics can be run either as a Lagrangian parcel model [*Connolly et al.*, 2009], or in a 1-D Eulerian framework with a discrete vertical resolution, as is the case for this study. The ACPIM microphysics has already been run within a 1-D column environment for the case of a precipitating idealized warm cloud [*Dearden et al.*, 2011] although the ACPIM has since been extended to include a treatment of the ice phase as well.

2.1. Microphysics

[8] With respect to the liquid phase, the ACPIM solves the diffusional growth equation [*Pruppacher and Klett*, 1997] to represent droplet activation and subsequent condensational growth. The Aerosol Diameter Dependent Equilibrium Model, ADDEM [*Topping et al.*, 2005a, 2005b] provides equilibrium vapor pressures of liquid particles, which are then fed into the droplet growth equation and solved in ACPIM such that the effects of specific particle compositions can be

explored in both liquid and mixed-phase clouds. Collision and coalescence processes are represented in ACPIM by solving the stochastic collection equation, although in this instance the sampled clouds were not observed to be precipitating. No riming is permitted in the model simulations by default; this is considered separately in a later section of this paper, where it is assumed that the rime mass is added as a spherical shell around the exterior of ice crystals, with a rime density equal to 200 kg m^{-3} based on the results of *Heymsfield and Pflaum* [1985]. Aggregation was found to play a negligible role in the model simulations.

[9] For ice nucleation, the scheme of *Koop et al.* [2000] is used to represent homogeneous freezing as a function of water activity of the solution droplets. In terms of heterogeneous nucleation, for this study the ACPIM uses the recent parameterization of *DeMott et al.* [2010], which determines ice crystal concentrations as a function of temperature and the number of aerosol particles greater than 500 nm thus:

$$N_{IN,T_K} = 0.0000594(273.16 - T_K)^{3.33} \times (n_{aer,0.5})^{(0.0264(273.16 - T_K) + 0.0033)}, \quad (1)$$

where T_K is the cloud temperature in Kelvin, $n_{aer,0.5}$ is the number concentration of particles with diameter larger than 500 nm (in std cm^{-3}) and N_{IN,T_K} is the IN number concentration (std L^{-1}) active at temperature T_K. The aerosol particle size distribution is initialized from in-situ measurements described later in section 3.

[10] The representation of depositional growth for ice in the ACPIM is based on the capacitance growth model described in *Chen and Lamb* [1994a], which is able to represent the evolution of ice crystal habit based on a consideration of the aspect ratio ϕ of spheroidal ice crystals, where $\phi = c/a$, c is the c-axis length and a is the a-axis length. Aspect ratios greater than 1 are prolate spheroids and correspond to columnar crystals, and values less than 1 are oblate spheroids describing plate-like crystals. In the adaptive parameterization of ice crystal habit, the change in mass of an ice crystal with time is given by the diffusional growth equation for ice:

$$\frac{dm}{dt} = \frac{4\pi C s_i}{\left[\frac{R_v T}{e_i D_v^*} + \frac{L_s}{T K_i^*}\left(\frac{L_s}{T R_v} - 1\right)\right]}, \quad (2)$$

where C is the crystal capacitance, specified in *Pruppacher and Klett* [1997] for both oblate and prolate spheroids; s_i is supersaturation with respect to ice, R_v is the vapor gas constant, L_s is the latent heat of sublimation, T is temperature, e_i is the equilibrium vapor pressure with respect to ice, D_v^* is the effective vapor diffusivity and K_i^* is the effective thermal conductivity. Equation (2) can also be expressed as a change in crystal volume dV, where

$$dV = \frac{1}{\rho_{dep}} dm, \quad (3)$$

and ρ_{dep} is the deposition density (the density of deposited vapor onto an ice crystal), and is expressed as (in g cm^{-3}):

$$\rho_{dep} = 0.91 \exp[-3.\max(\Delta\rho - 0.05, 0)/\Gamma(T)], \quad (4)$$

where $\Delta\rho$ is the excess vapor density in g m^{-3}, and Γ is the inherent growth ratio which controls the distribution of mass deposition onto the basal (c-axis) and prism (a-axis) faces of the crystal according to the ratio of the deposition coefficients α along the two axes:

$$\Gamma(T) = \frac{\alpha_c}{\alpha_a}. \quad (5)$$

Γ thus determines the primary habit evolution; it is a function of temperature and was determined by Chen and Lamb from both experimental data and in-situ observations across a range of temperatures between 0°C and -30°C [*Chen and Lamb*, 1994a, Figure 3].

[11] The dependency between the change in aspect ratio ϕ and the change in crystal volume V is given by:

$$d\ln(\phi) = \frac{\Gamma - 1}{\Gamma + 2} d\ln(V). \quad (6)$$

Equation (6) can be obtained from the volume of a spheroid $V = \frac{4}{3}\pi a^3 \phi$ and the assumption of a mass distribution relationship which controls the rate of crystal growth along each axis, such that:

$$\frac{dc}{da} = \Gamma(T)\Phi, \quad (7)$$

where Φ is the ratio of the vapor density gradients along the c and a axes, respectively. Equations (3) and (6) are solved in ACPIM to allow for changes in aspect ratio to feed back on ice crystal growth rates. Thus through the Chen and Lamb approach, the ACPIM is able to provide an adaptive representation of ice crystal density and aspect ratio, such that the growth and habit of ice crystals can respond to changing thermodynamic conditions while also accounting for their prior growth history. As noted recently [*Sheridan et al.*, 2009], relatively few numerical simulations of cold clouds have focused on predicting changes in aspect ratios and the effect this has on the evolution of ice crystal size distributions. Indeed, the effect of ice crystal habits in terms of cloud evolution and in particular, precipitation, are known to be profound [*Mason*, 1994], and so this is a potentially important feature of the model. Furthermore, the nucleation mechanism is known to affect the density, aspect ratio and growth rates of ice crystals [e.g., *Bacon et al.*, 2003, Table 1], and so the prognostic treatment is particularly appropriate when simulating clouds where both homogeneous and heterogeneous nucleation are possible.

[12] Fall speeds are calculated as a function of the area ratio of ice crystals, based on the recent findings of *Heymsfield and Westbrook* [2010]. This was shown to

improve computed fall speeds for particles of different habits relative to laboratory measurements. The area ratio is defined as the ratio of the projected area of the ice crystal to that of a circumscribing circle whose diameter is given by the maximum dimension of the ice crystal. The projected area for monomer ice crystals depends on their aspect ratio. Specifically, for plates (aspect ratios less than 1), the projected area is given by the area of a circle with radius equal to the *a*-axis length, and for columns (aspect ratios greater than 1) it is equal to that of an ellipse with semi-minor axis equal to the *a*-axis length and semi-major axis equal to the *c*-axis length.

2.2. Representation of Bin Structure

[13] The ACPIM uses a constant aerosol mass grid such that the aerosol bins are fixed (consistent with a single-moment representation), with 154 bins representing the aerosol size distribution. Both liquid and ice particle distributions are represented using a 2-D grid as in *Bott* [2000], such that particle number concentrations are categorized according to both water mass and aerosol mass. Thus for a given water mass bin, the 2-D grid stores the variation in number concentration across the range of aerosol mass bins, and vice versa. This allows for changes in the spectrum of aerosol mass to be simulated due to collisions between droplets. It is important to note that in this study, in contrast to the single-moment mass grids used in the method of Bott, the ACPIM is configured to use a double-moment 'moving center' bin structure to describe the evolution of both liquid and ice size distributions over time [*Jacobson*, 2005], such that the center of the mass bins are allowed to vary between the low and high bin edges. This is based on the latest developments to the ACPIM model described in *Connolly et al.* [2012], who showed that numerical diffusion during growth by vapor diffusion and collision-coalescence processes is reduced considerably with double-moment bin structures compared to single-moment solutions.

[14] Vertical advection of potential temperature and water vapor is handled using the positive definite, monotonic scheme of *Bott* [1992], where the polynomial interpolation is extended to 8th order [*Costa and Sampaio*, 1997]. Because a variable mass grid is used to describe the evolution of liquid and ice size distributions, the average mass within a given bin is not necessarily constant with height and so a different advection scheme must be used in this case. Consequently the dual-moment hybrid binning scheme is used for vertical advection of liquid and ice [*Chen and Lamb*, 1994b]. All simulations are performed with 320 levels in the vertical, and a fixed vertical resolution of 15 m with diagnostic output available every ten seconds.

3. Initialization of the Model

[15] Due to the one dimensional Eulerian nature of the driver model, vertical profiles of total water and potential temperature constrained from the observations are required to initialize the model and provide the basis of a realistic environment within which to study the formation and evolution of the wave cloud. However, at any given time, observations of the wave cloud only exist at a single height level, corresponding to the altitude of the flight track. Thus to obtain the initial profiles, the back trajectory method as employed in *Field et al.* [2012] is used, with the assumption that the flow is adiabatic such that total water and potential temperature are conserved along streamlines. By advecting the observations backwards in time along streamlines according to the measured vertical velocity (with all microphysical processes disabled), it is possible to obtain a vertical profile at the time corresponding to the start of the aircraft run from which the model can be run forwards (with microphysics enabled) to provide simulations of the wave cloud for further study.

[16] The procedure entails taking the measured time series of vertical velocity from the aircraft along a given flight track, and subsequently reversing and inverting it. The reversed vertical velocity field is then applied across all vertical model levels equally, with the implicit assumption that the vertical velocity field as measured by the aircraft is constant with height across the model domain, which covers a height of 4.8 kilometers (although the resultant clouds that form have considerably smaller depths than this, with an average liquid cloud depth of 1 km across the whole range of clouds sampled [*Heymsfield et al.*, 2011]). The model level closest to the flight level at the end of the aircraft run is initialized with the corresponding observations at that time. Prognostic variables are then advected backwards in time from the end of the run to the start of the run according to the reversed velocity time series, and should an advected air parcel intercept the flight level at some earlier time, the model is updated with the corresponding observations. This procedure leads to the production of the vertical profiles of potential temperature and total water used to initialize the model. Constraining the model in this manner in accordance with the in-situ measurements can be thought of as a basic form of data assimilation. In practice the method can sometimes lead to discontinuities of streamlines along the flight level, and thus it is necessary to include a small offset to the vertical velocity field when performing the back trajectories to ensure that the fields of potential temperature and total water follow continuous streamlines. The addition of an offset to the vertical velocity is justified because of the uncertainty in the absolute measurements from the aircraft.

[17] The ACPIM model also requires initialization in terms of the particle composition and size distribution. In terms of hygroscopic growth of the aerosol particles, the equilibrium behavior for specific aerosol chemical components are parameterized in the ACPIM model as a function of diameter based on results from the Aerosol-Diameter-Dependent-Equilibrium Model (ADDEM) [*Topping et al.*, 2005a, 2005b] thus allowing for the effects of composition on the growth rate of droplets to be accounted for. The study of *Pratt et al.* [2010] analyzed the residues of both cloud droplets and cloud ice in RF03 and identified the dominant presence of playa (dry lake bed) salts. Further

evaluation of the ability of the playa salts to act as CCN was conducted in the same study, with the conclusion that the playa salts have a relatively high hygroscopicity and a CCN efficiency close to that of sea-salt. With this in mind, the ACPIM model runs were configured to use pure sea-salt as the most suitable proxy for playa salts, although the strong dynamical forcing of the wave clouds meant that the model results were not found to be sensitive to this choice. With regards aerosol spectra, a time-mean size distribution from the Ultra-High Sensitivity Aerosol Spectrometer (UHSAS) probe was used to construct two fitted log-normal modes which are in turn used as inputs to the model (see Figure 1). The UHSAS size distribution was formed by averaging over the period between 20:42 UTC and 21:36 UTC, when the potential temperature range matched that of the sampled cloud.It should be noted that the UHSAS only produced reliable measurements in the range 0.1-1 μm, and so data below 100 nm was ignored when producing the log-normal fits (although it is assumed that the fitted modes continue to smaller sizes). Since the wave clouds are quite strongly forced, the model was found to activate all the available aerosol particles as cloud droplets, producing a typical droplet number concentration of 100 cm^{-3} which is consistent with the in-situ measurements.

[18] The number of particles present greater than 500 nm in diameter is particularly important as this controls the predicted ice crystal concentration in the model parameterization of heterogeneous ice nucleation. For the time-mean UHSAS data, the particle number greater than 500 nm is 0.116 cm^{-3} (with an uncertainty range of 0.09-0.14 cm^{-3} based on the Poisson sampling error), compared with 0.128 cm^{-3} for the fitted modes combined. Thus the fitted modes are safely within the uncertainty range of the measurements.

4. RF03: Flight Details

[19] In the field campaign, several straight and level passes were made through the cloud to characterize the evolution of the cloud microphysics as a function of altitude and time (see Figure 2). The labeling system for the straight and level runs is of the form *flight number-cloud number-penetration number*, e.g. 3-2-1 corresponds to the first penetration of the second cloud sampled on RF03. Measurements were first taken near the base of the liquid cloud and subsequent passes were made at higher levels in the cloud, finishing with measurements near cloud top. The typical horizontal wind speed through the wave cloud was 20 ms^{-1}, with the aircraft flying into the wind.

[20] By performing simulations of the wave cloud corresponding to different straight and level runs, it is possible to build up an understanding of the influence of both heterogeneous and homogeneous freezing in this particular case, and how the competition between the two ice nucleation mechanisms affects the ice crystal concentration at varying altitudes through the cloud

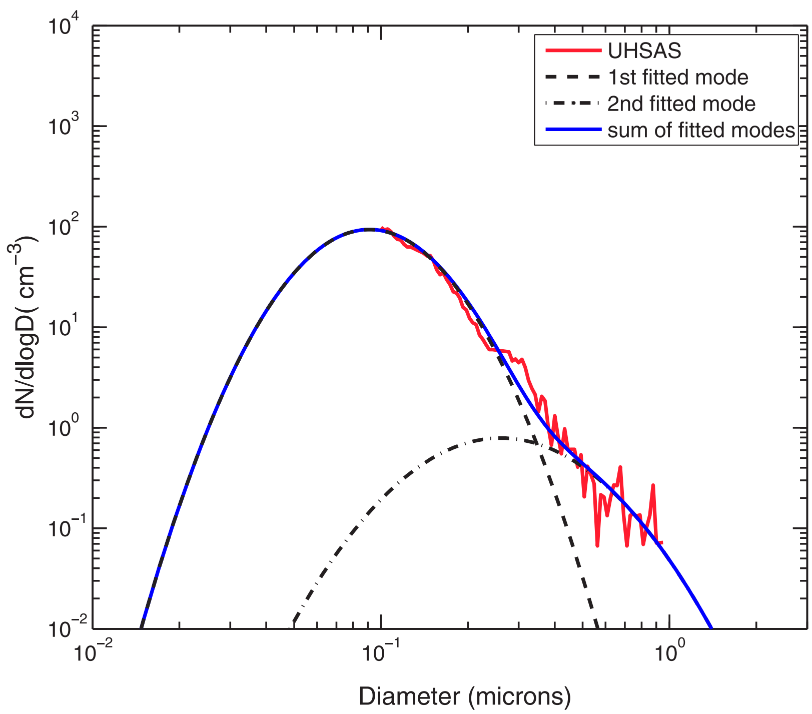

Figure 1. Time-mean UHSAS particle size distribution for RF03 (red); the fits to the UHSAS data used to initialize the model (black), and the summation of the two fitted modes (blue). Log-normal parameters for the first fitted mode (black dashed line) are: number concentration = 100 cm^{-3}; geometric mean diameter = 0.0911 μm; geometric standard deviation = 1.532. For the second mode (black dot-dashed line): number concentration = 1.125 cm^{-3}; geometric mean diameter = 0.26 μm; geometric standard deviation = 1.768.

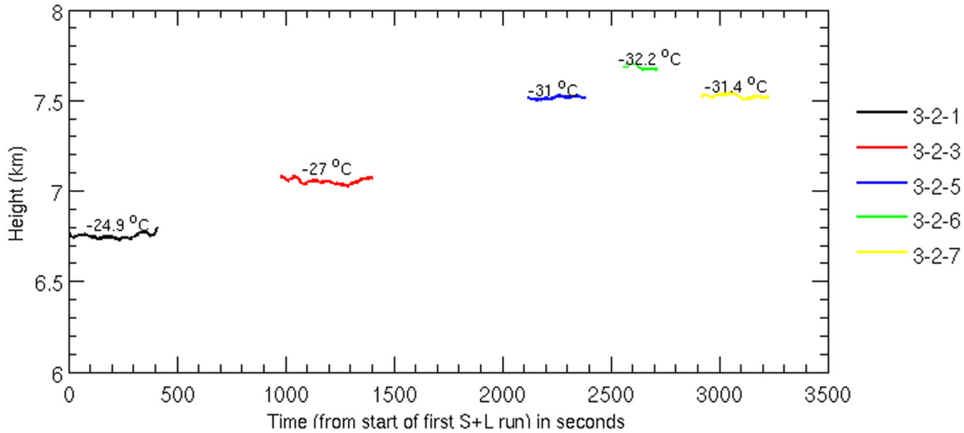

Figure 2. Time series of the straight and level runs (based on aircraft time) for RF03, corresponding to different heights above sea level through the evolution of the cloud. In-situ observations were taken along each run for the indicated duration. The average temperatures along each straight and level run are also indicated.

depth. When producing the initial vertical profiles in order to initialize the ACPIM model, the simulation of 3-2-3 was found to require a very large vertical velocity offset (+0.8 ms^{-1}) in order to eliminate discontinuities in streamlines. With this is mind it was decided to focus on penetrations 3-2-1, 3-2-5 and 3-2-7 for the basis of the modeling work, where the corresponding velocity offsets are considerably lower (+0.2 ms^{-1}, +0.3 ms^{-1} and +0.0 ms^{-1} respectively). Simulations of 3-2-6 are not considered since parcel trajectories for this particular penetration were not found to reach cold enough temperatures to be influenced by homogeneous freezing. The vertical velocity time series used to initialize the model relative to the in-situ measurements are plotted in Figure 3 in terms of air parcel time, obtained by multiplying the observation time by the ratio of the aircraft ground speed to the horizontal wind speed. The peak vertical velocity measured by the aircraft for this particular case was 3 ms^{-1}.

5. Model Results

5.1. Control Simulations: The Effect of Homogeneous Freezing

[21] This section shows results from model control simulations produced using a deposition coefficient of unity, and a prognostic treatment of ice density based on the Chen & Lamb model assuming an initial density of pure ice (910 kg m^{-3}). The time-height plots shown in Figure 4 illustrate the presence of both the liquid and ice phases, along with the corresponding temperature field, for the simulation of penetration 3-2-5. The closest model level to the flight track (based on the pressure level of the aircraft transit) is marked with a dashed black line. It can be seen that the model produces a cloud in response to the rising and cooling of air parcels in a manner that is consistent with the dynamical forcing shown in Figure 3. Once liquid droplets form in the simulation, the cloud very quickly evolves into a mixed-phase regime as the DeMott parameterization starts to produce ice (this is confirmed later in Figure 7). With homogeneous freezing disabled, the coldest temperature at which liquid droplets were simulated was −37°C and heterogeneous ice was produced throughout the depth of the cloud, with ice mass steadily increasing with time as the ice grows by deposition in the supersaturated environment.

[22] It can be seen how the cloud persists in a mixed-phase state up to approximately 1200 s into the simulation. At this time the vertical velocities are strongly negative, causing air parcels to descend and warm, leading to evaporation of the remaining liquid droplets. Beyond this time only an ice-tail remains, and parcel trajectories intercept the flight level at multiple points. In the case with both homogeneous and heterogeneous freezing enabled, it can be seen that considerably more ice mass is produced earlier on at cloud top from homogeneous nucleation. Soon after the liquid cloud forms, parcel trajectories reach temperatures cold enough to initiate the homogeneous freezing process. Analysis of the ice crystal number concentrations in the upper regions of the simulated cloud suggest that at most, 14% of the liquid droplets freeze homogeneously. As the vertical velocities become weaker in the transition from the updraft to the downdraft region of the wave, the in-cloud vapor pressure is no longer sufficient to sustain the remaining liquid droplets in the upper region of the liquid cloud and rapid glaciation occurs via the Wegener-Bergeron-Findeisen (WBF) process. Immediately downwind of the liquid cloud the ice contours in Figure 4 show a noticeable increase in ice mass crossing the flight level due to the effect of homogeneous freezing. Thus the influence of homogeneous freezing is clearly important in this particular simulation. A consideration of Figure 5 reveals that similar conclusions are reached for the simulation of 3-2-7; the influence of homogeneous freezing in the simulation of 3-2-1 is also apparent in Figure 5 but appears to be somewhat weaker than the other two cases. This is a consequence of liquid water only reaching −35.3°C in this simulation, and it is not clear from the contours whether enough homogeneously nucleated ice reaches the flight level to significantly influence the

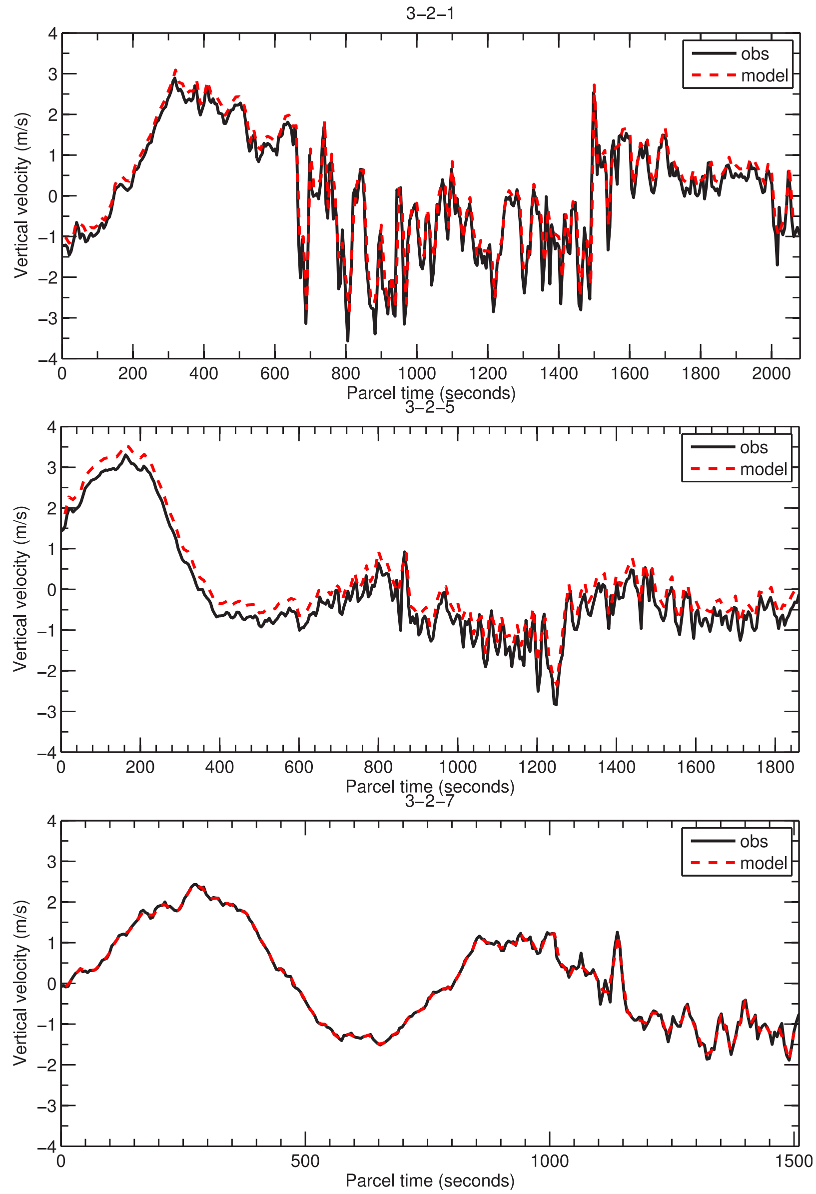

Figure 3. Vertical velocity fields used to initialize the model relative to the in-situ observations. The vertical velocity is constant with height in the model domain, i.e. applied equally at each model level. Any offsets from the measured values were necessary to avoid discontinuities in parcel streamlines during the model initialization process.

predicted ice concentration. To undertake a more rigorous analysis of the model performance, diagnostics along the flight track level must be compared directly to the available in-situ observations.

5.2. Comparison of Control Simulations With Observations

[23] Figure 6 compares time series of the predicted ice concentration in m^{-3} from the model control simulations with the corresponding in-situ measurements from the 'fast' 2D-C cloud probe, for penetration 3-2-5. The 2D-C used in the ICE-L field campaign benefits from upgraded photodiodes which minimizes sampling errors compared to earlier 2D-C probes [*Field et al.*, 2012]. The predicted concentrations from the model are taken from the closest model level to the flight track, i.e. along the black dashed line in Figure 4. The concentrations in both cases are restricted to a consideration of those ice crystals larger than 125 μm. This lower limit was chosen to reduce uncertainty in the sample volume of the probe below this size. While the use of a minimum size threshold is likely to underestimate the total ice crystal concentration, the same threshold is used when counting the predicted concentrations from the model to ensure a meaningful comparison. The results from both simulations (i.e. with and without homogeneous freezing) are shown together on the same plot.

[24] Initially the measurements show a steady increase in ice crystal concentration along the flight track; since the temperature along the flight track within the liquid

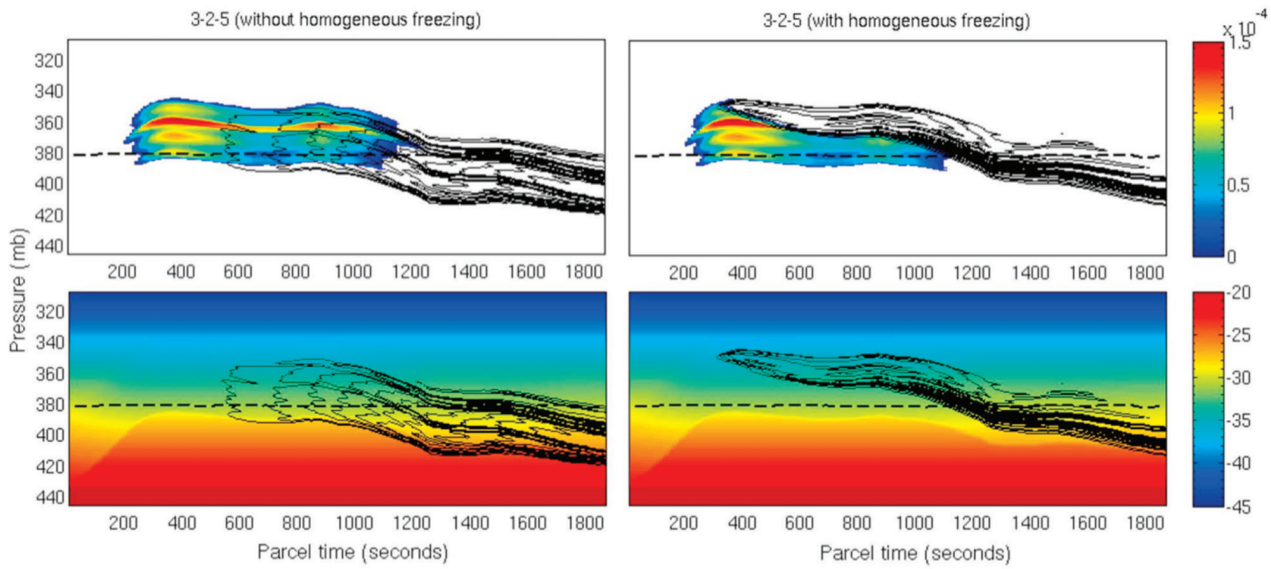

Figure 4. (top) Time-height contour plots from 3-2-5: liquid mass in kg kg^{-1} (colors) and ice mass in kg kg^{-1} (contours) for cases with homogeneous freezing both off and on (heterogeneous freezing is enabled in both cases). (bottom) The corresponding temperature in degrees Celsius (colors), with ice mass contours overlaid. The dashed black line in the plots denotes the closest model level to the aircraft flight track. The same number of ice contours are used (ten) for both sets of model runs, thus they are an indicator of where the majority of the ice mass is contained in each run and does not necessarily represent the same amount of ice in each case.

cloud does not change by more than 0.5°C this is unlikely to be explained by temperature-dependent nucleation (although as discussed in *Heymsfield et al.* [2011], this does not rule out the possibility that nucleation is time-dependent). However, the model maintains a more constant ice crystal concentration along the flight track, and the detection of ice above 125 μm is slightly later than in the measurements. The DeMott parameterization produces an active IN concentration of around 1 L^{-1}, which compares well to the average measured IN concentrations of 1 L^{-1} for RF03, with a maximum of 3 L^{-1} and a standard deviation of 0.7 L^{-1} as stated in *Pratt et al.* [2010]. Around 900 s parcel time there is a much larger jump in the observed ice crystal concentration, which the model simulation without homogeneous freezing is not able to reproduce. From 1200 s however too many ice crystals persist above 125 μm in the model, whereas the observations show a distinct drop in concentration. When homogeneous freezing is permitted to occur in the model (dashed blue line in Figure 6), the agreement with the observations improves, at least in a qualitative sense, with the model now able to produce a distinct ice tail, although it occurs too late compared to the observations and also overestimates. However, the rapid reduction in ice crystal concentration above 125 μm that follows is well captured by the model; this can be explained through consideration of the relative humidity plot in Figure 7. The effect of homogeneously nucleated ice in the upper regions of the cloud is to increase the sink of supersaturation such that by the time the air descends and warms in the descending part of the wave, the relative humidity is considerably lower than it otherwise would be. Consequently this reduction in relative humidity leads to sublimation of the ice crystals in the subsaturated air and hence reduces the number of ice crystals above the 125 μm size threshold. Thus treatment of the homogeneous freezing process in the model is necessary not only to explain the peaks in observed ice crystal concentration, but also to explain the reduction in ice concentration above 125 μm downstream of the ice tail by virtue of competition for the available water vapor. Figure 7 also reveals some interesting features with regards the effect of homogeneous freezing on the predicted aspect ratio and density of the ice crystals in the model. When homogeneous freezing is enabled, the onset of the ice tail coincides with a sudden change in both the aspect ratio and the ice crystal density. The reduction in the aspect ratio signifies a change in the properties of the ice population from a mainly columnar habit to more spherical ice crystals. This is indicative of a regime change from heterogeneously nucleated ice to a population that is dominated by homogeneously nucleated crystals, which individually exhibit less growth (and therefore an overall lower aspect ratio) than their heterogeneously nucleated counterparts. Similar findings can be reached through consideration of the ice density diagnostic, where the model shows an increase in the density of ice crystals due to the influence of homogeneous ice intercepting the flight track. These conclusions are consistent with ice crystal images from the Cloud Particle Imager (CPI) probe, an analysis of which reveals that the ice crystals sampled within the ice tail region were generally smaller, more spherical and denser than those in the mixed-phase regime (see Figure 8). This demonstrates that a prognostic treatment of ice density in models is advantageous for

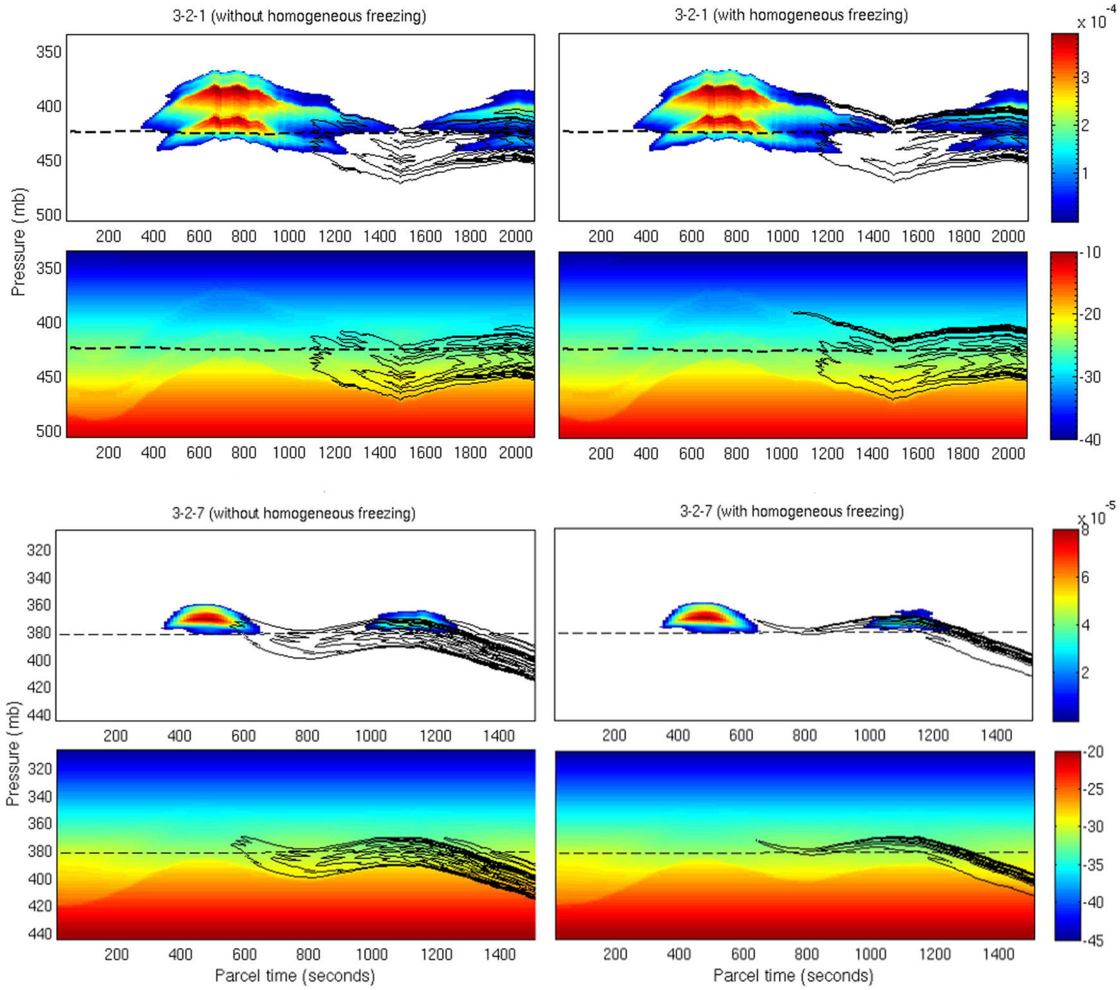

Figure 5. As Figure 4 but for simulations of (top) 3-2-1 and (bottom) 3-2-7.

characterizing the microphysics of clouds where both homogeneous and heterogeneous nucleation are important sources of ice. The predicted ice water content is underestimated relative to the calculated value from the 2D-C measurements, although it must be noted that the observed ice water content is derived assuming spherical

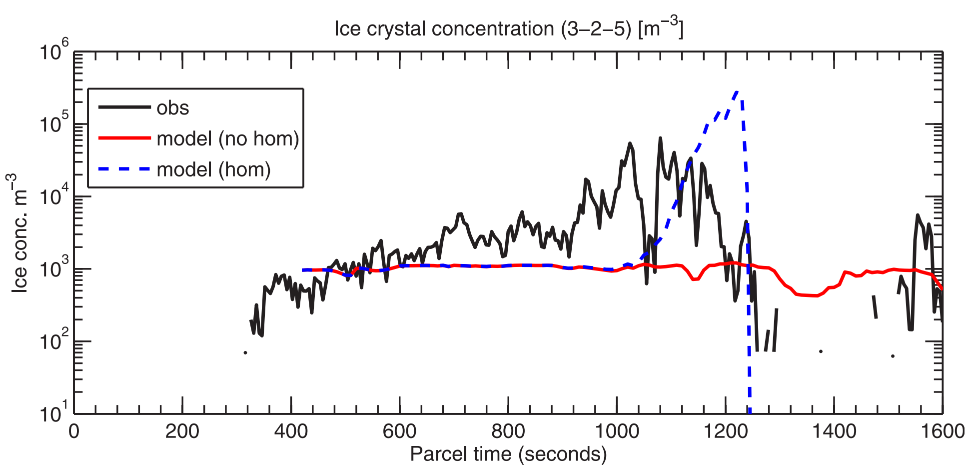

Figure 6. Observed ice crystal concentrations (m^{-3}) for sizes larger than 125 μm compared against those predicted by the model control simulations for the 3-2-5 flight track. The observed concentrations in all cases are taken from measurements using the 'fast' 2D-C probe as discussed in the text.

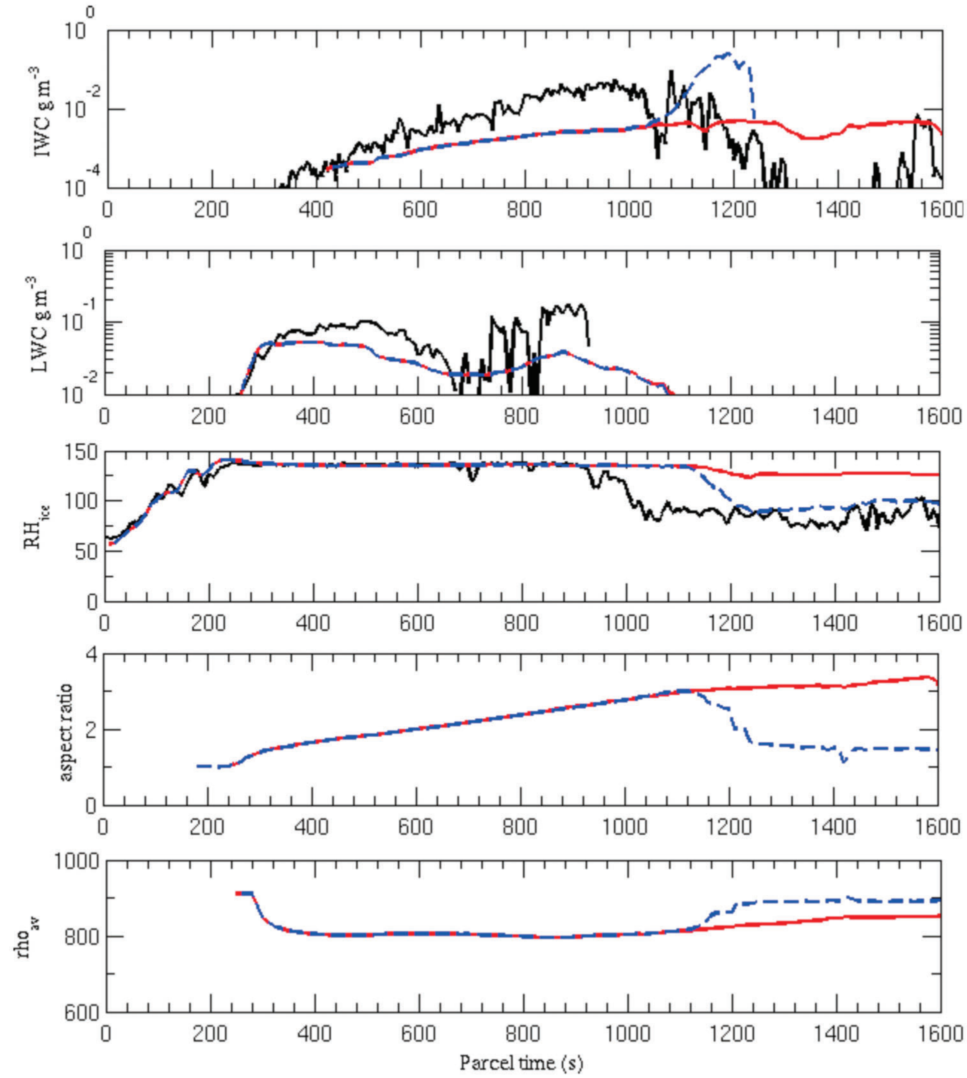

Figure 7. Additional flight level diagnostics for 3-2-5, comparing predicted values from the model with the observations where possible. The observations are in black while the model results are in blue (with homogeneous freezing) and red (without homogeneous freezing). From top downward: ice water content in g m^{-3}, with observations derived from integrated 2D-C data assuming spherical ice and constant density of 100 kg m^{-3} based on the findings of *Heymsfield et al.* [2011]; liquid water content in g m^{-3}, with observed values from the King liquid water content probe; relative humidity with respect to liquid; predicted average aspect ratio of ice crystals from the model; predicted average density of ice crystals from the model (kg m^{-3}).

ice and a constant bulk density of 100 kg m^{-3}. This bulk density is based on results from *Heymsfield et al.* [2011, Figure 18b], who showed that an effective ice density of 100 kg m^{-3} or less is necessary to account for the observed growth rates of heterogeneously nucleated ice crystals in ICE-L wave clouds. The study by *Heymsfield et al.* [2011] shows that the effective ice density reduces below 100 kg m^{-3} at larger crystal sizes, and so the assumption of a constant value may lead to an over-estimation of the calculated ice water content in Figure 7. Note that the liquid water content also appears to be underestimated; the implications of this are explored later in this section.

[25] The comparison of the predicted ice crystal concentration with the observations for penetrations 3-2-1 and 3-2-7 are shown in Figure 9. The influence of homogeneous freezing along the flight track in the simulation of 3-2-1 appears to be very small, and results in no noticeable improvement when compared with the observations. This is a consequence of the fact that liquid droplets are only exposed to a minimum temperature of −35.3°C for this particular simulation, and so the amount of homogeneously nucleated ice produced is much lower than in the other simulated cases. This may be a result of the assumption that the vertical winds are constant with altitude in the model simulation. For instance, it is possible that the vertical winds may have been stronger aloft compared to the magnitude at the sampling altitude, although this cannot be proven. For 3-2-7, Figure 9 shows that

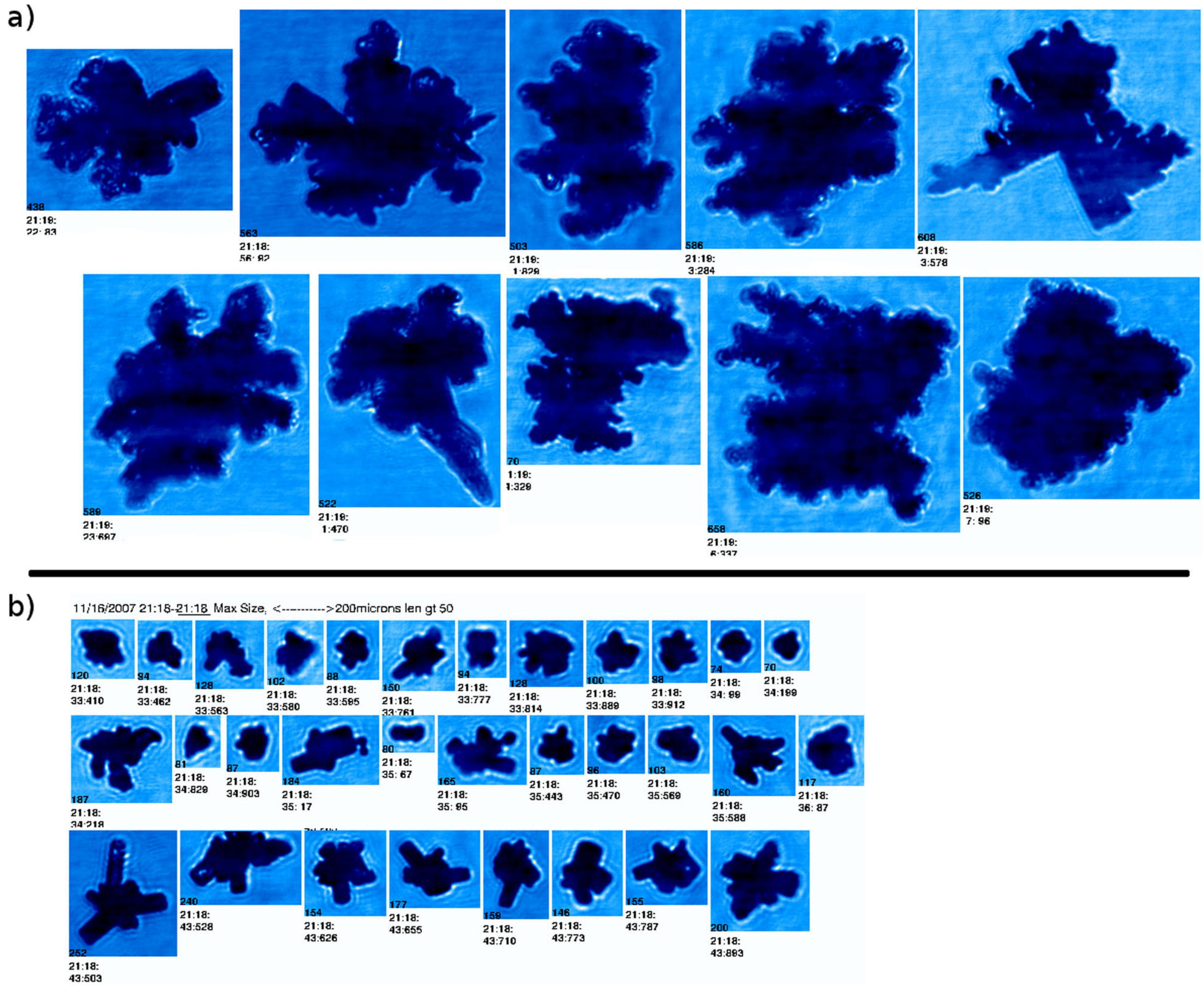

Figure 8. Example images of ice crystals from the CPI probe observed along penetration 3-2-5. (a) A sample of ice crystals detected within the liquid cloud region, showing a few heavily rimed ice crystals. (b) A sample of ice crystals detected in the ice tail region of the cloud. Analysis of CPI data for penetrations 3-2-1 and 3-2-3 revealed similar evidence of rimed ice crystals in the liquid cloud region only.

homogeneous freezing has more of an influence on the predicted ice crystal concentration along the flight track as suggested by Figure 5, but the peaks do not coincide with those seen in the observations. The parcel trajectories in Figure 5 suggest that homogeneous freezing takes place too close to the flight level in the model simulation, producing anomalous peaks in ice crystal concentration associated with homogeneous freezing in the liquid cloud regime and an ice tail that peaks too early. It can be argued that given the limitations of the vertical wind measurements in relation to variations with height, it is justifiable to consider adjacent model levels within the vicinity of the flight track location to see if the agreement between the predicted and observed values can be improved. In the case of 3-2-7 the simulation of ice crystal concentrations relative to the available observations was improved by considering the predicted values 100 m below the flight level (not shown), although it was not possible to do so without compromising other aspects of the simulation (specifically ice water content and relative humidity).

[26] In the simulation of penetration 3-2-5 however, this approach is more successful and highlights a potentially important conclusion that is worthy of further comment. Figure 10 plots the predicted ice concentrations from 3-2-5 approximately 100 m above the flight level plotted in Figure 4, revealing an increase in ice crystal concentrations within the liquid cloud that are more consistent with those seen in the measurements. The improvement in the predicted concentrations around 700 s parcel time can be explained by falling homogeneously nucleated ice crystals from above in a time period when the vertical velocities are weakly negative. This is a potentially important result since it means that the ice crystal concentrations along certain penetrations of the observed liquid cloud may have contained non-negligible concentrations of homogeneously nucleated ice, which

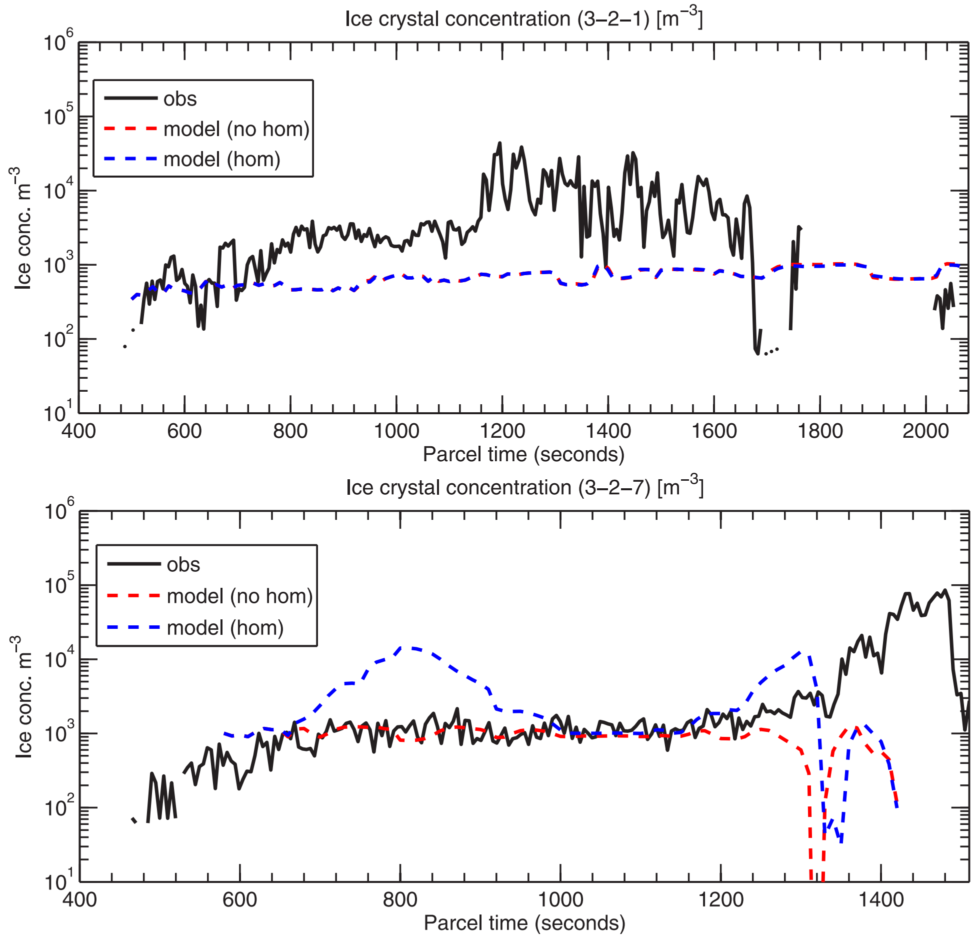

Figure 9. As Figure 6 but for penetrations (top) 3-2-1 and (bottom) 3-2-7.

may have led to slight overestimates of IN concentrations for this particular cloud in the modeling study of *Field et al.* [2012]. The onset of the ice tail is better simulated as well, although the subsequent decrease in ice crystal concentrations above 125 μm occurs too abruptly. It is possible, given the underestimation of liquid water content as shown in Figure 7, that the simulation also underestimates the amount of liquid water near cloud top as well, such that during the WBF process the ice crystals are unable to grow quite as large as in the

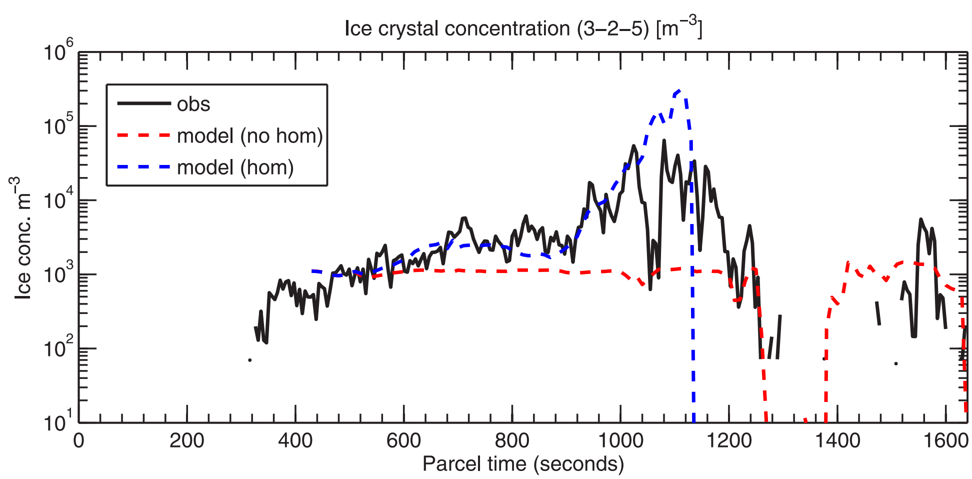

Figure 10. Comparison of the observed and predicted ice crystal concentrations for penetration 3-2-5, where the predicted concentrations are shown along a trajectory approximately 100 m above the position of the aircraft altitude level. Simulations use prognostic ice density, with both homogeneous freezing off (red) and on (blue).

observations. However, we cannot rule out the possibility that the inherent growth ratio used in the model (which is based on laboratory measurements down to only −30°C) may not be appropriate at colder temperatures, particularly where homogeneous nucleation occurs. It is unfortunate that it was not possible to explore in more detail the influence of homogeneous freezing in penetration 3-2-1 due to the apparent uncertainty in the forcing conditions leading to insufficient homogeneous nucleation in this simulation. This at least serves as a reminder of how small discrepancies in dynamic factors can have significant consequences for the accuracy of the simulation of the cloud microphysics.

5.3. The Effect of Riming

[27] In an effort to understand the source of the few heavily rimed crystals seen in the observations (see Figure 8), additional simulations were performed with the riming process included, thus permitting collisions between liquid and ice particles to act as a sink of liquid and a source of ice mass. Simulations of both 3-2-1 and 3-2-5 with riming enabled were performed for cases both with and without homogeneous freezing; in all cases the riming efficiency (i.e. the probability of a liquid droplet sticking to an ice crystal upon contact) was taken to be unity. For clarification, only collisions between liquid and ice cloud particles were accounted for; collisions between liquid drops only (accretion) and ice crystals only (aggregation) were found to be negligible and thus were not considered in the simulations. In these simulations, the stochastic collection equation was solved based on the number and mass conserving method of moments. The average rime mass per ice crystal from the simulations of 3-2-1 and 3-2-5 are shown in Figure 11.

[28] It is clear from Figure 11 that in both cases, the average amount of rime mass per ice crystal is reduced considerably in the absence of homogeneous nucleation. Thus the additional source of ice from homogeneous freezing was found to increase the efficiency of the riming process. Additional simulations were also performed for 3-2-1 where the total number of aerosol particles with diameter less than 500 nm was doubled, while the number concentration of particles larger than 500 nm (i.e. the potential number of IN) was left unchanged. This resulted in an approximate doubling of the cloud droplet number concentration in the cloud to 200 cm^{-3}, and the effect of the smaller droplets was to reduce the average rime mass per ice crystal by as much as a factor of five. This result is qualitatively consistent with the study of *Borys et al.* [2003], who observed that riming rates are reduced in orographic wave clouds due to a reduction in cloud droplet size under a fixed liquid water content.

[29] In the simulation of 3-2-5, although the overall amount of rimed ice produced is less than in the simulation of 3-2-1, the rimed ice crystals are closer to the flight track level. In particular, for 3-2-5 the simulated rimed crystals are closest to the aircraft altitude between 700–900 s parcel time, and with the aforementioned uncertainty in the model vertical wind field taken into account, it is possible to conceive that rimed ice could intercept the flight level at this time. This would certainly explain the presence of the few heavily rimed ice crystals seen in the in-situ observations within the liquid cloud. It should be remembered when interpreting these results that the concentrations of homogeneously nucleated ice are likely to be underestimated in the simulations of 3-2-1, and as such more liquid water is potentially available for riming in the upper regions of the cloud relative to the simulation of 3-2-5. As discussed in section 5.1, the weakening updraught speeds during the transition from positive to negative vertical velocities, coupled with the higher concentrations of homogeneous ice in 3-2-5, allow the WBF process to become more effective at removing the remaining droplets in the upper regions of the cloud. Consequently dynamical factors were found to be important in determining the amount of rimed ice produced in the model simulations through the ability to regulate the role of the WBF mechanism.

5.4. Additional Sensitivity Tests With the Factorial Method

[30] Having considered the performance of the model in the context of the in-situ measurements, the results of some additional sensitivity tests are now presented in relation to exploring the susceptibility of the model simulation to changes in selected microphysical variables. The paper by *DeMott et al.* [2010] states that active IN concentrations must be accurate to within a factor of ten in cloud and climate models in order to prevent significant discrepancies arising in the simulation of cloud properties, from both a microphysical and radiative perspective. Since the DeMott parameterization of active IN concentration is a function of both particle number greater than 500 nm and temperature, this scheme in conjunction with the ACPIM model can be used to test the sensitivity of the wave cloud to changes in aerosol particle number concentration, with the aim of establishing how important the representation of the aerosol particle size distribution is in terms of the impact on microphysical processes in these types of clouds. To assess the model sensitivity in this regard, the Factorial Method (FM) is employed, which has been used previously in the context of cloud modeling [*Teller and Levin*, 2008; *Dearden et al.*, 2011] to quantify the relative importance of selected microphysical variables to changes in a chosen metric. The FM is particularly useful as it can isolate and quantify the non-linear dependencies between specific variables, which can be significant for ice phase microphysics. For this particular case, the FM is applied to quantify the extent to which an increase in the number of particles available to act as IN affects the overall ice crystal concentration through the competition with homogeneous ice nucleation. It is also worthy of remembrance at this point that all the model simulations thus far have assumed a deposition coefficient of unity, but this quantity is known to be uncertain for ice [*Pruppacher and Klett*, 1997, p. 165; *Gierens et al.*, 2003]. Indeed lower values of the deposition coefficient could slow the growth rate of ice by deposition, thus

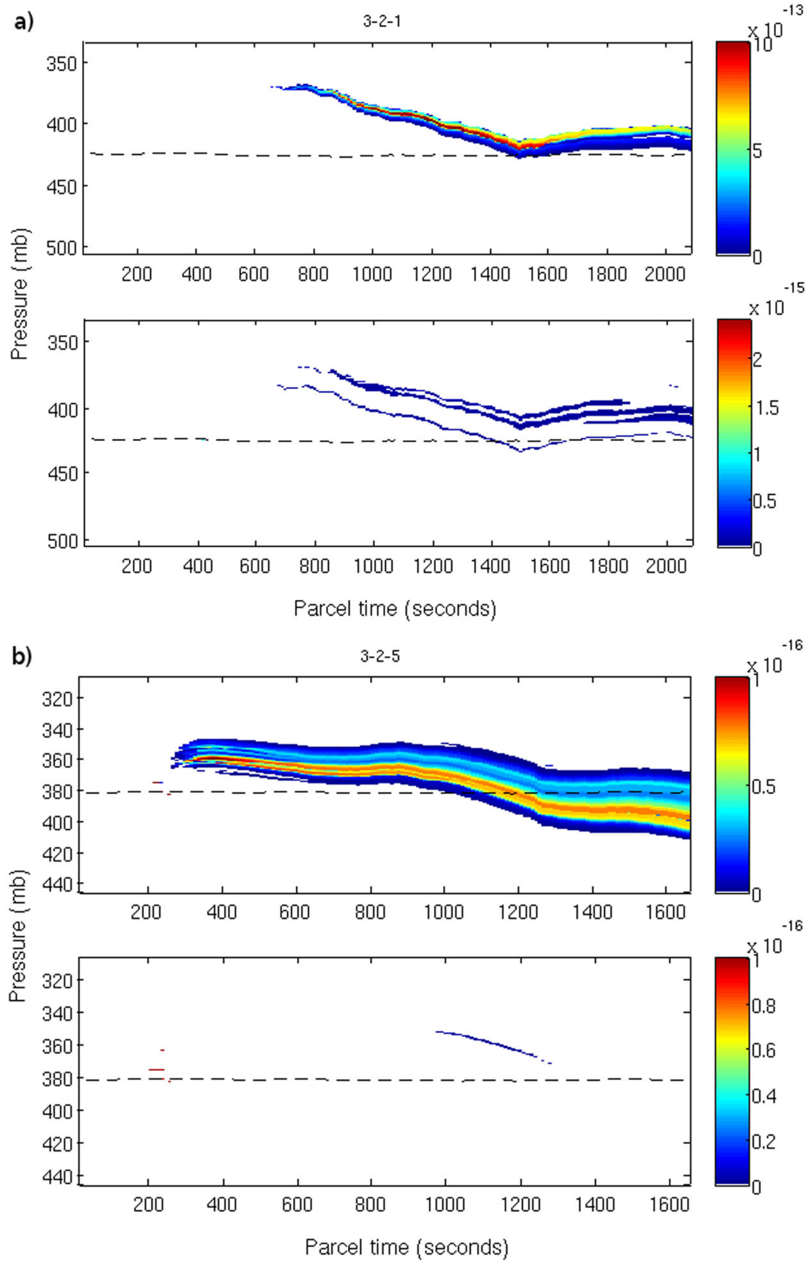

Figure 11. Contour plots of average rimed mass per ice crystal (kg kg^{-1}) from simulations of (a) 3-2-1 and (b) 3-2-5. In each case, the top plot corresponds to simulations with both heterogeneous and homogeneous freezing enabled; the bottom plot shows results from simulations with just heterogeneous nucleation of ice permitted. The black dashed line indicates the position of nearest model level to the flight track.

reducing the sink of supersaturation and potentially maintaining a higher level of supersaturation for longer such that it may have a non-negligible effect on homogeneous freezing rates. Recent laboratory estimates for the deposition coefficient in cirrus clouds suggest a value between 0.1 and 1.0 [*Skrotzki et al.*, 2010]. Thus the effect of the uncertainty in the value of the deposition coefficient is also taken into account in the experimental design of the FM.

[31] Three factors are chosen for study, with two values assigned to each factor, yielding a 2^3 factorial design such that eight model simulations are required. Specifically, the factors considered are the role of homogeneous freezing (labeled *A*), the value of the deposition coefficient (*B*), and the number concentration of potential IN (*C*). The values assigned to each factor along with the experimental design matrix are tabulated in Tables 1 and 2 respectively. For each factor, the 'low' and 'high' values are designated such that the transition from low to high would be expected to increase the ice crystal concentration at some point along the flight track. The DeMott parameterization represents the potential number of available IN as those aerosol particles greater than 500 nm in diameter. By reducing

Table 1. Chosen Factors and the Values Assigned to Them Based on a 2^3 Factorial Design

Factor Label	Factor Description	Values
A	The effect of homogeneous freezing	Off; On
B	The value of the deposition coefficient	1.0; 0.1
C	The aerosol particle size threshold representing number of potential IN	500 nm; 300 nm

this threshold from 500 nm to 300 nm, the number of potential IN increases from a concentration of 0.11 cm^{-3} to 1.0 cm^{-3}, approximately an order of magnitude increase, as shown in Figure 12.

[32] The FM analysis was applied to simulations where the influence of homogeneous freezing was appreciable, namely 3-2-5 and 3-2-7, with similar conclusions for each case. Figure 13 shows the results of the Factorial Method analysis for simulations of 3-2-7, specifically the average effect of each factor (*A*, *B* and *C*), with the individual interaction terms (*AB*, *AC*, *BC*, *ABC*) that represent the competition between factors on a separate axis. Considering the main effects first, the dominant variable in terms of the effect on the ice crystal concentration along the flight track is the effect of homogeneous freezing, shown in blue. The effect of increasing the number of potential IN leads to an increase in heterogeneous ice of around 2 L^{-1}, while the average effect of the change in deposition coefficient from 1.0 to 0.1 appears to be the least important of the three factors considered. The dominant interaction terms seem to be between *AB* and *AC*, representing the susceptibility of the homogeneous freezing process to the changes in deposition coefficient and IN concentration respectively. Where the effect of *AB* is negative, this shows that the effect of homogeneous freezing reduces in response to the lowering of the deposition coefficient from 1.0 to 0.1. Similar conclusions are reached for the interaction *AC*, the case when the IN concentration is increased. However, Figure 13 shows that the magnitude of the interaction terms are considerably smaller than the main effects; indeed, in terms of the overall contribution to the change in ice crystal concentration, the interaction terms typically explain no more than 10% of the total variance. This means that the specified changes to the deposition coefficient and the assumed IN concentration have a relatively small impact on the homogeneous freezing process, and that for the range of values tested, the specified microphysical factors do not have a particularly strong dependence on each other. If the cloud were more weakly forced initially such that the magnitude of the updraughts were smaller when ice was first formed, it is possible to conceive that competition between microphysical factors could have a more significant impact on the model predictions of ice crystal concentration. For example, if the vapor pressure in cloud at the time of heterogeneous ice formation was less than the equilibrium vapor pressure over water but greater than that over ice at a given temperature, then heterogeneously nucleated ice would grow at the expense of liquid droplets through the WBF process, therefore reducing the potential number of liquid droplets in the cloud available for homogeneous freezing. However, as noted in the study by *Korolev* [2007], the WBF process is more likely to be disabled in clouds with stronger updraughts, where the in-cloud vapor pressure can be high enough to prevent the liquid droplets from evaporating in the presence of ice crystals. Such conclusions are not dissimilar to those of *Karcher and Lohmann* [2003] in the context of cirrus clouds, who suggested that, depending

Table 2. The Experimental Design Matrix for the 2^3 Design Used in This Study[a]

Run Label	Value of *A*	Value of *B*	Value of *C*
(*one*)	Off	1.0	500 nm
a	On	1.0	500 nm
b	Off	0.1	500 nm
ab	On	0.1	500 nm
c	Off	1.0	300 nm
ac	On	1.0	300 nm
bc	Off	0.1	300 nm
abc	On	0.1	300 nm

[a]The run labels follow the convention of 'standard notation,' whereby the presence of a lower case letter denotes the high value of that factor, and the absence of a lowercase letter indicates the low value of that factor. For example, run *ab* corresponds to the model simulation where factors *A* and *B* are at the 'high' level, and *C* is at the 'low' level. The label (*one*) is reserved for the simulation when all three factors are at the low level.

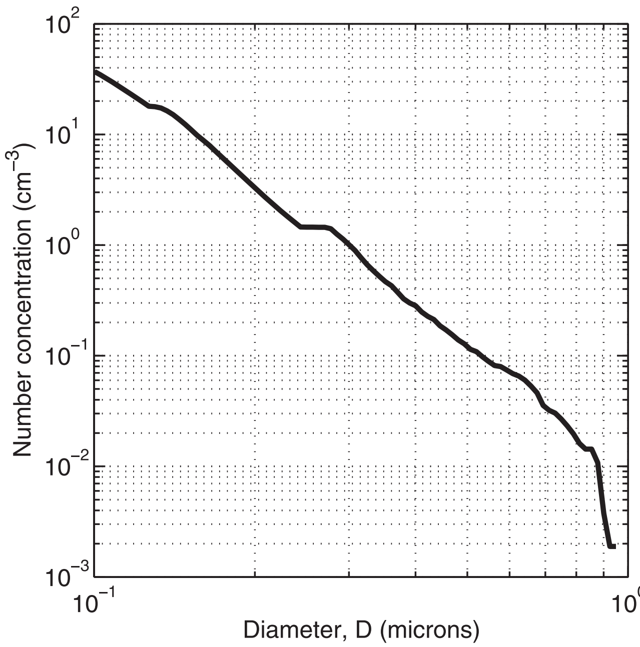

Figure 12. Cumulative number concentration of aerosol particles above a given size threshold, from UHSAS measurements of RF03. The cumulative concentration is plotted in cm^{-3} for diameters between 0.1 and 1.0 μm.

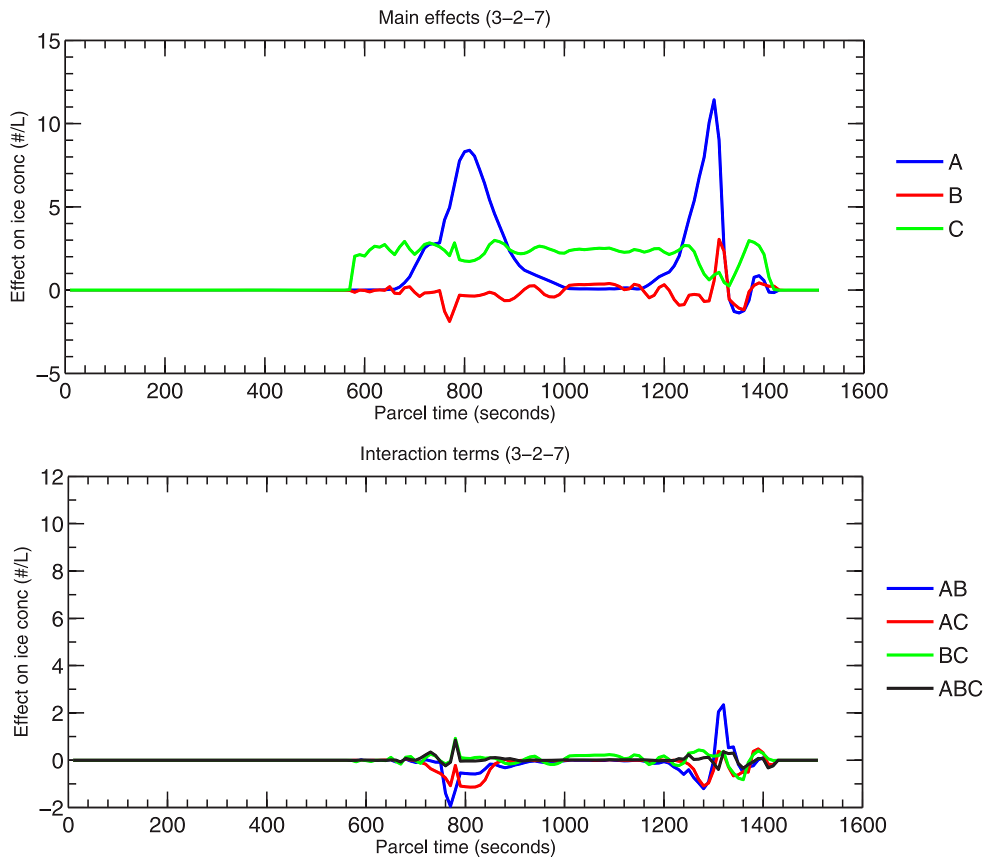

Figure 13. Time series plots from the Factorial Method analysis, showing (top) the average effects of each factor and (bottom) the effects of interactions between factors in terms of the induced change in predicted ice crystal concentration above 125 μm along the flight track. The two-factor interactions represent the competition between: homogeneous freezing and the deposition coefficient (*AB*), homogeneous freezing and the IN concentration (*AC*) and finally the deposition coefficient and IN concentration (*BC*). The remaining three-factor interaction (*ABC*) represents the dependency of the *AB* interaction on the value of *C*.

on the dynamical forcing conditions, increases in IN concentration can lower the overall ice crystal concentration in cirrus through competition with, and possibly even suppression of, the homogeneous freezing process.

6. Summary and Conclusions

[33] This study has sought to explain the measurements of ice crystal concentration from an ICE-L wave cloud using a detailed microphysics model embedded within a 1-D column framework. The study has focused on the role of interactions between heterogeneous and homogeneous freezing in accounting for the in-situ observations of ice crystal number, and has also considered more subtle features such as the ability of the model to explain the origin of heavily rimed particles seen in images of ice crystals sampled in-situ.

[34] The use of a prognostic treatment of ice density was shown to be advantageous for simulating changes in aspect ratio and density along the flight track in response to the presence of both heterogeneous and homogeneously nucleated ice. Homogeneously nucleated ice was produced in all the model simulations of the chosen wave cloud, and although it did not always intercept the simulated flight level in the model, the limitations of the model forcing must be taken into account here. The initialization of the model is based on in-situ data available at a single penetration through the cloud at any one time, coupled with the assumption that the vertical velocity is the same above and below the flight track level for the whole model domain. While this was found to have little impact on the predicted ice concentrations associated with heterogeneous nucleation, this was found to be more of an issue when considering the influence of homogeneous nucleation, which is highly sensitive to the representation of liquid water content and cloud top temperature. The dynamical forcing was also found to play a role in determining the amount of liquid water available for riming in the model simulations. After homogeneous nucleation occurs, the in-cloud updraught speeds become weaker in the transition from positive to negative vertical velocities, and this causes the remaining droplets in the upper region of the cloud to evaporate in the presence of the homogeneous ice crystals as a result of the Bergeron-Findeisen process. This rapid glaciation imposes a limit on the amount of riming possible, although the results from the model simulations suggest that a limited amount of rimed ice could still intercept the

flight level within the liquid cloud regime, which is qualitatively consistent with the detection of a few heavily rimed ice crystals in the in-situ observations.

[35] In cases where the predicted ice crystal concentrations along the flight track were clearly affected by homogeneous freezing, it was possible to conduct additional sensitivity studies based around the Factorial Method (FM) to explore the effect of changes in the deposition coefficient and the potential number of IN in the model. The results of the FM analysis show that the peaks in ice crystal concentration arising from homogeneous nucleation were relatively robust to changes in the chosen microphysical factors. The strong dynamical forcing of the cloud in question should be taken into account when considering this result, as this has the potential to overshadow the competition between homogeneous and heterogeneous ice formation to some extent. Since the vertical velocities measured during RF03 are fairly typical of those encountered during the ICE-L field campaign as a whole, it is possible to suggest that for wave clouds where both homogeneous and heterogeneous freezing processes are active, model errors associated with the number concentration of large aerosol particles are likely to have less of an effect on the simulation of the cloud microphysical processes compared to more weakly forced clouds, where the competition between the two distinct pathways of primary ice nucleation is likely to be more important through the effects of the Bergeron-Findeisen process. This suggests that dynamical considerations should be taken into account when considering the extent to which the effect of aerosols need to be represented in microphysics schemes, and that such an approach may help to optimize the balance between microphysical complexity and computational cost in the future development of ice phase microphysics parameterizations for use in larger scale models.

[36] Given the relative microphysical complexity of the RF03 case compared to other ICE-L wave clouds, it is encouraging that the modeling results shown in this paper can help to understand and explain particular features of the in-situ measurements. It is likely that any discrepancies between the predicted and observed ice crystal concentrations have arisen from the limitations of the observational constraints used to initialize the model, as opposed to deficiencies in the model microphysics. However, it is worthy of note that the observations of the wave cloud in this study stretch to lower temperatures than those considered by existing laboratory studies of ice growth rates, such as those by *Takahashi and Fukuta* [1988]. Thus it may be useful to extend such laboratory studies to temperatures where the observations we report here have been taken.

[37] **Acknowledgments.** The first author would like to thank the ICE-L team for their permission to use the ICE-L data set, and in particular Aaron Bansemer at NCAR for processing the CPI data. This work was funded by NERC studentship reference NE/F00821X/1.

References

Bacon, N. J., M. B. Baker, and B. D. Swanson (2003), Initial stages in the morphological evolution of vapour-grown ice crystals: A laboratory investigation, *Q. J. R. Meteorol. Soc.*, *129*(591), 1903–1927, doi:10.1256/qj.02.04.

Borys, R. D., D. H. Lowenthal, S. A. Cohn, and W. O. J. Brown (2003), Mountaintop and radar measurements of anthropogenic aerosol effects on snow growth and snowfall rate, *Geophys. Res. Lett.*, *30*(10), 1538, doi:10.1029/2002GL016855.

Bott, A. (1992), Monotone flux limitation in the area-preserving flux-form advection algorithm, *Mon. Weather Rev.*, *120*(11), 2592–2602, doi:10.1175/1520-0493(1992)120<2592:MFLITA>2.0.CO;2.

Bott, A. (2000), A flux method for the numerical solution of the stochastic collection equation: Extension to two-dimensional particle distributions, *J. Atmos. Sci.*, *57*(2), 284–294, doi:10.1175/1520-0469(2000)057<0284:AFMFTN>2.0.CO;2.

Cantrell, W., and A. Heymsfield (2005), Production of ice in tropospheric clouds: A review, *Bull. Am. Meteorol. Soc.*, *86*(6), 795–807, doi:10.1175/BAMS-86-6-795.

Chen, J. P., and D. Lamb (1994a), The theoretical basis for the parameterization of ice crystal habits: Growth by vapor-deposition, *J. Atmos. Sci.*, *51*(9), 1206–1221, doi:10.1175/1520-0469(1994)051<1206:TTBFTP>2.0.CO;2.

Chen, J. P., and D. Lamb (1994b), Simulation of cloud microphysical and chemical processes using a multicomponent framework: 1. Description of the microphysical model, *J. Atmos. Sci.*, *51*(18), 2613–2630, doi:10.1175/1520-0469(1994)051<2613:SOCMAC>2.0.CO;2.

Connolly, P. J., O. Moehler, P. R. Field, H. Saathoff, R. Burgess, T. Choularton, and M. Gallagher (2009), Studies of heterogeneous freezing by three different desert dust samples, *Atmos. Chem. Phys.*, *9*(8), 2805–2824, doi:10.5194/acp-9-2805-2009.

Connolly, P. J., C. Emersic, and P. R. Field (2012), A laboratory investigation into the aggregation efficiency of small ice crystals, *Atmos. Chem. Phys.*, *12*, 2055–2076, doi:10.5194/acp-12-2055-2012.

Cooper, W. A. (1986), Ice initiation in natural clouds: Precipitation enhancement—A scientific challenge, *Meteorol. Monogr.*, *21*, 29–32, doi:10.1175/0065-9401-21.43.29.

Costa, A. A., and A. J. C. Sampaio (1997), Bott's area-preserving flux-form advection algorithm: Extension to higher orders and additional tests, *Mon. Weather Rev.*, *125*(8), 1983–1989, doi:10.1175/1520-0493(1997)125<1983:BSAPFF>2.0.CO;2.

Dearden, C., P. J. Connolly, T. W. Choularton, and P. R. Field (2011), Evaluating the effects of microphysical complexity in idealised simulations of trade wind cumulus using the Factorial Method, *Atmos. Chem. Phys.*, *11*(6), 2729–2746, doi:10.5194/acp-11-2729-2011.

DeMott, P. J., A. J. Prenni, X. Liu, S. M. Kreidenweis, M. D. Petters, C. H. Twohy, M. S. Richardson, T. Eidhammer, and D. C. Rogers (2010), Predicting global atmospheric ice nuclei distributions and their impacts on climate, *Proc. Natl. Acad. Sci. U. S. A.*, *107*(25), 11,217–11,222, doi:10.1073/pnas.0910818107.

Eidhammer, T., et al. (2010), Ice Initiation by Aerosol Particles: Measured and Predicted Ice Nuclei Concentrations versus Measured Ice Crystal Concentrations in an Orographic Wave Cloud, *J. Atmos. Sci.*, *67*(8), 2417–2436, doi:10.1175/2010JAS3266.1.

Field, P. R., et al. (2008), Contrasting the ice nucleation in two lee wave clouds observed during the ICE-L campaign, paper presented at 15th International Conference on Clouds and Precipitation, Int. Comm. on Clouds and Precip., Cancun, Mexico.

Field, P. R., A. J. Heymsfield, B. J. Shipway, P. J. DeMott, K. A. Pratt, D. C. Rogers, J. Stith, and K. A. Prather (2012), Ice in Clouds Experiment-Layer Clouds. Part II: Testing characteristics of heterogeneous ice formation in lee wave clouds, *J. Atmos. Sci.*, *69*(3), 1066–1079, doi:10.1175/JAS-D-11-026.1.

Fletcher, N. H. (1962), *Physics of Rain Clouds*, Cambridge Univ. Press, London.

Gierens, K., M. Monier, and J. Gayet (2003), The deposition coefficient and its role for cirrus clouds, *J. Geophys. Res.*, *108*(D2), 4069, doi:10.1029/2001JD001558.

Heymsfield, A. J., and J. C. Pflaum (1985), A quantitative assessment of the accuracy of techniques for calculating graupel growth, *J. Atmos. Sci.*, *42*(21), 2264–2274, doi:10.1175/1520-0469(1985)042<2264:AQAOTA>2.0.CO;2.

Heymsfield, A. J., and C. D. Westbrook (2010), Advances in the estimation of ice particle fall speeds using laboratory and field measurements, *J. Atmos. Sci.*, *67*(8), 2469–2482, doi:10.1175/2010JAS3379.1.

Heymsfield, A. J., P. R. Field, M. Bailey, D. Rogers, J. Stith, C. Twohy, Z. Wang, and S. Haimov (2011), Ice in Clouds Experiment-Layer Clouds. Part I: Ice growth rates derived from lenticular wave cloud penetrations, *J. Atmos. Sci.*, *68*(11), 2628–2654, doi:10.1175/JAS-D-11-025.1.

Jacobson, M. K. (2005), *Fundamentals of Atmospheric Modeling*, 2nd ed., Cambridge Univ. Press, New York.

Karcher, B., and U. Lohmann (2003), A parameterization of cirrus cloud formation: Heterogeneous freezing, *J. Geophys. Res.*, *108*(D14), 4402, doi:10.1029/2002JD003220.

Khain, A., A. Pokrovsky, M. Pinsky, A. Seifert, and V. Phillips (2004), Simulation of effects of atmospheric aerosols on deep turbulent convective clouds using a spectral microphysics mixed-phase cumulus cloud model. Part I: Model description and possible applications, *J. Atmos. Sci.*, *61*(24), 2963–2982, doi:10.1175/JAS-3350.1.

Koop, T., B. P. Luo, A. Tsias, and T. Peter (2000), Water activity as the determinant for homogeneous ice nucleation in aqueous solutions, *Nature*, *406*(6796), 611–614, doi:10.1038/35020537.

Korolev, A. (2007), Limitations of the wegener-bergeron-findeisen mechanism in the evolution of mixed-phase clouds, *J. Atmos. Sci.*, *64*(9), 3372–3375, doi:10.1175/JAS4035.1.

Mason, B. J. (1994), The shapes of snow crystals: Fitness for purpose? *Q. J. R. Meteorol. Soc.*, *120*(518), 849–860, doi:10.1256/qj.02.04.

Meyers, M. P., P. J. Demott, and W. R. Cotton (1992), New primary ice-nucleation parameterizations in an explicit cloud model, *J. Appl. Meteorol.*, *31*(7), 708–721, doi:10.1175/1520-0450(1992)031<0708:NPINPI>2.0.CO;2.

Pratt, K. A., et al. (2010), Observation of playa salts as nuclei in orographic wave clouds, *J. Geophys. Res.*, *115*, D15301, doi:10.1029/2009JD013606.

Pruppacher, H. R., and J. D. Klett (1997), *Microphysics of Clouds and Precipitation*, Kluwer Acad., Boston, Mass.

Seifert, A., A. Khain, A. Pokrovsky, and K. D. Beheng (2006), A comparison of spectral bin and two-moment bulk mixed-phase cloud microphysics, *Atmos. Res.*, *80*(1), 46–66, doi:10.1016/j.atmosres.2005.06.009.

Sheridan, L. M., J. Y. Harrington, D. Lamb, and K. Sulia (2009), Influence of ice crystal aspect ratio on the evolution of ice size spectra during vapor depositional growth, *J. Atmos. Sci.*, *66*(12), 3732–3743, doi:10.1175/2009JAS3113.1.

Skrotzki, J., P. Connolly, M. Niemand, H. Saathoff, O. Moehler, V. Ebert, and T. Leisner (2010), The accommodation coefficient of water molecules on ice: Results from cirrus cloud experiments at the aerosol chamber AIDA, Abstract A21F-0171 presented at 2010 Fall Meeting, AGU, San Francisco, Calif., 13–17 Dec.

Takahashi, T., and N. Fukuta (1988), Supercooled cloud tunnel studies on the growth of snow crystals between $-4°C$ and $-20°$, *J. Meteorol. Soc. Jpn.*, *66*(6), 841–855.

Teller, A., and Z. Levin (2008), Factorial method as a tool for estimating the relative contribution to precipitation of cloud microphysical processes and environmental conditions: Method and application, *J. Geophys. Res.*, *113*, D02202, doi:10.1029/2007JD008960.

Topping, D. O., G. B. McFiggans, and H. Coe (2005a), A curved multi-component aerosol hygroscopicity model framework: Part 1. Inorganic compounds, *Atmos. Chem. Phys.*, *5*, 1205–1222, doi:10.5194/acp-5-1205-2005.

Topping, D. O., G. B. McFiggans, and H. Coe (2005b), A curved multi-component aerosol hygroscopicity model framework: Part 2. Including organic compounds, *Atmos. Chem. Phys.*, *5*, 1223–1242, doi:10.5194/acp-5-1223-2005.

Westbrook, C. D., and A. J. Illingworth (2011), Evidence that ice forms primarily in supercooled liquid clouds at temperatures $> -27°C$, *Geophys. Res. Lett.*, *38*, L14808, doi:10.1029/2011GL048021.

Corresponding author: C. Dearden, School of Earth, Atmospheric and Environmental Science, University of Manchester, Simon Building, Oxford Road, Manchester M13 9PL, UK. (christopher.dearden@manchester.ac.uk)